Electronic Supplementary Information (ESI)

A new family of thiolate-bridged bimetallic complexes featuring benzimidazole moiety: synthesis, structure and redox reactivity

Kai Di,[a] Dawei Yang,*[a] Linan Su,[a] Ronghuan Du,[a] Shengbin Dong,[b] Baomin Wang[a] and Jingping Qu*[a,b]

[a]*State Key Laboratory of Fine Chemicals, Frontier Science Center for Smart Materials, Dalian University of Technology, Dalian 116024, P. R. China.*
[b]*State Key Laboratory of Bioreactor Engineering, Collaborative Innovation Centre for Biomanufacturing, Frontiers Science Center for Materiobiology and Dynamic Chemistry, East China University of Science and Technology, Shanghai 200237, P. R. China.*

E-mail: qujp@dlut.edu.cn; yangdw@dlut.edu.cn

Table of Contents

I. General Materials and Methods.....3

II. Experimental Procedures and Analytical Data 5

III. X-ray Crystallographic Data.....8

IV. NMR Spectra.....16

V. IR Spectra 18

VI. ESI High-resolution Mass Spectra 21

VII. Cyclic Voltammograms 25

VIII. *In situ* ^{1}H NMR Spectra 27

IX. UV/vis Spectra.....28

X. Computational Details 31

XI. References.....33

I. General Materials and Methods

General Procedures

All manipulations were performed under an argon or nitrogen atmosphere by standard Schlenk techniques or in a Braun (Germany) or Mikrouna (China) glove box maintained at or below 1 ppm of O_2 and H_2O unless otherwise specified. All solvents were dried and distilled over an appropriate drying agent under an argon or nitrogen atmosphere. Benzimidazolylmethyl disulfide (bzmds), benzimidazol-2-ylmethanethiol (bzmt),[1] $[Cp^*Fe(MeCN)_3][PF_6]$ ($Cp^* = \eta^5$-C_5Me_5),[2] $[Cp^*CoI_2(CO)]$,[3] $[Cp^*Ru(MeCN)_3][PF_6]$,[4] graphite potassium (KC_8),[5] and ferricenium hexafluorophosphate ($FcPF_6$)[6] were prepared according to literature procedures. Reagents NaOAc, KPF_6, and Na_2SO_4 are commercially available and used as received without further purification.

Spectroscopic Measurements

^1H NMR spectra is recorded on a Brüker 400 Ultra Shield spectrometer. The chemical shifts (δ) are given in parts per million relative to CD_3CN (1.94 ppm for ^1H), CD_2Cl_2 (5.32 ppm for ^1H). Infrared spectra were recorded on a NEXVSTM FT-IR spectrometer. Electrospray ionization high-resolution mass spectra were recorded on a Q-Tof Micro. Elemental analyses were performed on a Vario EL analyzer. Electrochemical measurements were recorded using a BAS-100W electrochemical potentiostat at a scan rate of 100 mV/s. Electrochemical experiments were carried out in a three-electrode cell under argon at room temperature. The working electrode was a glassy carbon disk (diameter 3 mm), the reference electrode was a nonaqueous $Ag/AgNO_3$ electrode, the auxiliary electrode was a platinum wire, and the supporting electrolyte was 0.1 M $^nBu_4NPF_6$ in MeCN. All potentials reported herein are quoted relative to the Fc/Fc^+ couple. Solution-phase magnetic measurements were performed by Evans' method.[7–10] UV/vis spectra were recorded on a Perkin Elmer Lambda 1050+ spectrometer.

X-ray Crystallography

Single-crystal X-ray diffraction studies were carried out on a Brüker SMART APEX

CCD diffractometer with graphite-monochromated Mo Kα radiation (λ = 0.71073 Å). Empirical absorption corrections were performed using the SADABS program.[11] All structures were solved by direct methods and refined by full-matrix least-squares procedures on F^2 using SHELXTL2014[12,13] and solved with the Superflip structure solution program using charge flipping and refined with the XL refinement package using least squares minimization that is included in Olex2.[14–16] All of the non-hydrogen atoms were refined anisotropically. All of the hydrogen atoms on carbons were generated and refined in ideal positions. CCDC depositions 2290813 (**1**), 2346393 (**2**) 2357272 (*syn*-**3**), 2346394 (*anti*-**3**), 2368460 (**4**) can be obtained free of charge from the Cambridge Crystallographic Data Center.

Computational Details

The PBE[17,18] functional in combination with the def2-TZVP[19] basis set were applied to geometry optimizations and the subsequent frequency analyses. The resolution of identity (RI)[20] approximation was employed to speed up the calculations. Moreover, the Becke−Johnson (D3BJ) damping was also utilized to take noncovlent corrections into account.[21]

II. Experimental Procedures and Analytical Data

Preparation of *syn*-[Cp*Fe(μ-1κ^2*SN*:2κ^1*S*-bzmt)]$_2$[PF$_6$]$_2$ (1)

Method A: Bzmds (43 mg, 0.13 mmol) was added to a MeCN solution (5 mL) of [Cp*Fe(MeCN)$_3$][PF$_6$] (119 mg, 0.26 mmol) at room temperature. The colour of the reaction mixture immediately changed from violet to yellow-brown. After being stirred for 1 h, the resultant solution was evaporated to dryness under vacuum. The solids were washed with *n*-hexane (3 mL × 3) to afford a yellow-brown powder **1** (110 mg, 0.11 mmol, 85%). Single-crystals suitable for X-ray diffraction analysis were obtained from a MeCN solution layered with Et$_2$O at room temperature.

Method B: FcPF$_6$ (36 mg, 0.11 mmol) was added to a THF solution (5 mL) of **4** (94 mg, 0.11 mmol) at room temperature. The colour of the reaction mixture immediately changed from green to yellow-brown. After being stirred for 30 min, the resultant solution was evaporated to dryness under vacuum. The solids were washed with *n*-hexane (3 mL × 3) to afford a yellow-brown powder **1** (91 mg, 0.091 mmol, 83%). Single-crystals suitable for X-ray diffraction analysis were obtained from a MeCN solution layered with Et$_2$O at room temperature.

^{1}H NMR (400 MHz, CD$_3$CN, ppm): δ 9.51 (s, 2H, N*H*), 7.31 (t, 2H, *J* = 7.6 Hz, Ph-*H*), 7.20 (t, 2H, *J* = 7.6 Hz, Ph-*H*), 6.95 (d, 2H, *J* = 4.1 Hz, Ph-*H*), 6.90 (d, 2H, *J* = 4.1 Hz, Ph-*H*), 4.46 (d, 2H, *J* = 9.5 Hz, C*H*$_2$), 3.70 (d, 2H, *J* = 9.5 Hz, C*H*$_2$), 1.38 (s, 30H, Cp*-C*H*$_3$). HRMS (ESI, *m/z*) calcd. for C$_{36}$H$_{44}$Fe$_2$N$_4$S$_2$ [**1**–2(PF$_6$)]$^{2+}$, 354.0854, found 354.0849. IR (Film, cm^{-1}): 3380 (ν_{NH}), 3190, 3121, 2990, 2916, 1626, 1458, 1377, 1274, 1017, 843, 754, 561. UV/vis [λ_{max} (nm), ε (M^{-1}cm^{-1})]: 279 (18852), 318 (10362), 394 (5896), 462 (3833). Anal. Calcd. for C$_{36}$H$_{44}$Fe$_2$N$_4$S$_2$P$_2$F$_{12}$: C, 43.30; H, 4.44; N, 5.61. Found: C, 43.10; H, 4.68; N, 5.65.

Preparation of *syn*-[Cp*Co(μ-1κ^2*SN*:2κ^1*S*-bzmt)]$_2$[PF$_6$]$_2$ (2)

To a precooled solution of [Cp*CoI$_2$(CO)] (362 mg, 0.76 mmol) in CH$_2$Cl$_2$:H$_2$O = 1:1 (20 mL) was added with NaOAc (1.246 g, 15.20 mmol), KPF$_6$ (1.398 g, 7.60 mmol)

and bzmt (125 mg, 0.76 mmol) were added at room temperature. The colour of the reaction mixture gradually changed from violet-red to red. After stirring at room temperature for 12 h, the organic phase was collected and the aqueous phase was washed with a small amount of CH_2Cl_2. The combined CH_2Cl_2 solution was dried over Na_2SO_4 and filtered. The filtrate was dried under vacuum and washed with *n*-hexane (10 mL × 3) to afford a red powder **2** (351 mg, 0.35 mmol, 92%). Single-crystals suitable for X-ray diffraction analysis were obtained from a CH_2Cl_2 solution layered with *n*-hexane at room temperature.

^{1}H NMR (400 MHz, CD_3CN, ppm): δ9.70 (s, 2H, N*H*), 7.57 (d, 2H, *J* = 3.8 Hz, Ph-*H*), 7.48 (t, 2H, *J* = 7.2 Hz, Ph-*H*), 7.38 (t, 2H, *J* = 7.2 Hz, Ph-*H*), 7.11 (d, 2H, *J* = 3.8 Hz, Ph-*H*), 3.45 (d, 2H, *J* = 9.0 Hz, C*H*$_2$), 3.06 (d, 2H, *J* = 9.0 Hz, C*H*$_2$), 1.43 (s, 30H, Cp*-C*H*$_3$). HRMS (ESI, *m/z*) calcd. for $C_{36}H_{44}Co_2N_4S_2$ [**2**–2(PF_6)]$^{2+}$, 357.0836, found 357.0827. IR (Film, cm^{-1}): 3364 (ν_{NH}), 2967, 2920, 1452, 1276, 1018, 841, 749, 558. UV/vis [λ_{max} (nm), ε (M^{-1}cm^{-1})]: 280 (22472), 367 (15054), 530 (2979). Anal. Calcd. for $C_{36}H_{44}Co_2N_4S_2P_2F_{12}$: C, 43.04; H, 4.41; N, 5.58. Found: C, 43.05; H, 4.90; N, 5.39.

Preparation of *syn*-[Cp*Ru(*μ*-1κ^2*SN*:2κ^1*S*-bzmt)]$_2$[PF_6]$_2$ (*syn*-3) and *anti*-[Cp*Ru(*μ*-1κ^2*SN*:2κ^1*S*-bzmt)]$_2$[PF_6]$_2$ (*anti*-3)

Bzmds (33 mg, 0.10 mmol) was added to a MeCN solution (15 mL) of [Cp*Ru(MeCN)$_3$][PF_6] (100 mg, 0.20 mmol) at room temperature. The colour of the reaction mixture immediately changed from orange-yellow to yellow-brown. After being stirred for 1 h, the resultant solution was evaporated to dryness under vacuum. The solids were extracted with THF (5 mL × 3) and dried under vacuum. The extracted solids were washed with *n*-hexane (3 mL × 3) to afford a yellow-brown powder *syn*-**3** (81 mg, 0.074 mmol, 74%). Single-crystals suitable for X-ray diffraction analysis were obtained from a CH_2Cl_2 solution layered with *n*-hexane at room temperature.

^{1}H NMR (400 MHz, CD_3CN, ppm): δ9.64 (s, 2H, N*H*), 7.37 (t, 2H, *J* = 7.5 Hz, Ph-*H*), 7.28 (t, 2H, *J* = 7.5 Hz, Ph-*H*), 7.05 (d, 2H, *J* = 4.1 Hz, Ph-*H*), 7.01 (d, 2H, *J* = 4.1 Hz, Ph-*H*), 4.06 (d, 2H, *J* = 9.5 Hz, C*H*$_2$), 3.42 (d, 2H, *J* = 9.5 Hz, C*H*$_2$), 1.77 (s, 30H, Cp*-

C*H*$_3$). IR (Film, cm^{-1}): 3390 (ν_{NH}), 2962, 2921, 2848, 1646, 1454, 1380, 1277, 1023, 840, 750, 559. UV/vis [λ_{max} (nm), ε (M^{-1}cm^{-1})]: 280 (22048), 369 (9910). Anal. Calcd. for $C_{36}H_{44}Ru_2N_4S_2P_2F_{12}$: C, 39.71; H, 4.07; N, 5.15. Found: C, 40.88; H, 4.47; N, 5.27.

The residual solids were washed with *n*-hexane (3 mL × 3) to afford a green powder *anti*-**3** (16 mg, 0.015 mmol, 15%). Single-crystals suitable for X-ray diffraction analysis were obtained from a MeCN solution layered with Et_2O at room temperature.

^{1}H NMR (400 MHz, CD_3CN, ppm): δ 10.97 (s, 2H, N*H*), 7.48−7.35 (8H, Ph-*H*), 4.45 (s, 4H, C*H*$_2$), 1.30 (s, 30H, Cp*-C*H*$_3$). HRMS (ESI, *m/z*) calcd. for $C_{36}H_{44}Ru_2N_4S_2$ [**3**–2(PF_6)]$^{2+}$, 400.0556, found 400.0555. IR (Film, cm^{-1}): 3382 (ν_{NH}), 2963, 2920, 2770, 1453, 1400, 1285, 1018, 841, 765, 558. UV/vis [λ_{max} (nm), ε (M^{-1}cm^{-1})]: 279 (19845), 319 (8983), 398 (7166). Anal. Calcd. for $C_{36}H_{44}Ru_2N_4S_2P_2F_{12}$: C, 39.71; H, 4.07; N, 5.15. Found: C, 39.44; H, 4.44; N, 4.96.

Preparation of *syn*-[Cp*Fe(μ-1κ^2*SN*:2κ^1*S*-bzmt)]$_2$[PF_6] (4)

KC_8 (34 mg, 0.25 mmol) was added to a THF solution (15 mL) of **1** (210 mg, 0.21 mmol) at −78 °C. The colour of the reaction mixture gradually changed from yellow-brown to green. The mixture was stirred and gradually warmed to ambient temperature. The resulting green solution was evaporated to dryness under reduced pressure. The residue was extracted with CH_2Cl_2 (5 mL × 3) and dried under vacuum to afford a green powder **4** (102 mg, 0.12 mmol, 57%). Single-crystals suitable for X-ray diffraction analysis were obtained from a CH_2Cl_2 solution layered with *n*-hexane at room temperature.

HRMS (ESI, *m/z*) calcd. for $C_{36}H_{44}Fe_2N_4S_2$ [**4**–PF_6]$^+$, 708.1708, found 708.1711. IR (Film, cm^{-1}): 3366 (ν_{NH}), 2963, 2921, 1627, 1455, 1377, 1021, 840, 754, 559. UV/vis [λ_{max} (nm), ε (M^{-1}cm^{-1})]: 278 (2534), 472 (252), 830(5). μ_{eff} (CD_2Cl_2, Evans' method, 25 ℃) = 1.50 ± 0.05 μ_B. Complex **4** is extremely sensitive to air and therefore cannot provide elemental analysis data.

III. X-ray Crystallographic Data

Table S1. Crystallographic data for **1**·MeCN and **2**·2CH_2Cl_2.

	1·MeCN	**2**·2CH2Cl2
Formula	$C_{38}H_{47}F_{12}Fe_2N_5P_2S_2$	$C_{38}H_{48}Cl_4Co_2F_{12}N_4P_2S_2$
Formula weight	1039.56	1174.52
Crystal dimensions (mm^3)	0.32×0.25×0.23	0.33×0.31×0.29
Crystal system	Triclinic	Monoclinic
Space group	P−1	$P2_1/n$
a (Å)	10.992(3)	11.5804(8)
b (Å)	11.940(4)	36.884(3)
c (Å)	17.155(5)	12.2830(9)
α (º)	92.109(3)	90
β (º)	101.285(3)	117.113(3)
γ (º)	102.490(3)	90
Volume ($Å^3$)	2148.2(11)	4670.0(6)
Z	2	4
T (K)	200.0	120.0
D_{calcd} (g cm^{-3})	1.607	1.671
μ (mm^{-1})	0.935	1.180
F (000)	1064.0	2384.0
No. of rflns. collected	16524	44435
No. of indep. rflns. /R_{int}	7423/0.0472,	8134/0.1427
No. of obsd. rflns. [$I_0 > 2\sigma(I_0)$]	5925	4801
Data / restraints / parameters	7423/228/616	8134/181/624
R_1 / wR_2 [$I_0 > 2\sigma(I_0)$]	0.0525/0.1505	0.0953/0.1797
R_1 / wR_2 (all data)	0.0672/0.1610	0.1610/0.2050
GOF (on F^2)	1.137	1.035
Largest diff. peak and hole (e $Å^{-3}$)	0.67/−0.65	0.81/−0.67
CCDC No.	2290813	2346393

Table S2. Crystallographic data for *syn*-**3**·CH_2Cl_2 and *anti*-**3**·2MeCN.

	syn-**3**·CH_2Cl_2	*anti*-**3**·2MeCN
Formula	$C_{37}H_{46}Cl_2F_{12}N_4P_2Ru_2S_2$	$C_{40}H_{50}F_{12}N_6P_2Ru_2S_2$
Formula weight	1173.88	1171.06
Crystal dimensions (mm^3)	0.27×0.25×0.22	0.29×0.27×0.23
Crystal system	Orthorhombic	Monoclinic
Space group	$P2_12_12_1$	$P2_1/n$
a (Å)	12.7973(18)	11.290(2)
b (Å)	16.870(2)	15.799(3)
c (Å)	20.971(3)	13.395(3)
α (º)	90	90
β (º)	90	110.230(5)
γ (º)	90	90
Volume ($Å^3$)	4527.4(11)	2241.9(8)
Z	4	2
T (K)	200.0	120.0
D_{calcd} (g cm^{-3})	1.722	1.735
μ (mm^{-1})	1.031	0.927
F (000)	2352.0	1180.0
No. of rflns. collected	53085	38133
No. of indep. rflns. /R_{int}	7928/0.0800	3936/0.1018
No. of obsd. rflns. [$I_0 > 2\sigma(I_0)$]	6208	3322
Data / restraints / parameters	7928/204/561	3936/0/295
R_1 / wR_2 [$I_0 > 2\sigma(I_0)$]	0.0610/0.1182	0.0408/0.0890
R_1 / wR_2 (all data)	0.0934/0.1253	0.0509/0.0955
GOF (on F^2)	1.131	1.072
Largest diff. peak and hole (e $Å^{-3}$)	1.86/−0.73	0.74/−0.57
CCDC No.	2357272	2346394

Table S3. Crystallographic data for **4**.

	4
Formula	$C_{36}H_{44}F_6Fe_2N_4PS_2$
Formula weight	853.54
Crystal dimensions (mm^3)	0.25×0.23× 0.22
Crystal system	Monoclinic
Space group	$P2_1/c$
a (Å)	17.5444(16)
b (Å)	14.6053(14)
c (Å)	14.6529(15)
α (º)	90
β (º)	95.899(2)
γ (º)	90
Volume ($Å^3$)	3734.8(6)
Z	4
T (K)	298.0
D_{calcd} (g cm^{-3})	1.518
μ (mm^{-1})	0.994
F (000)	1764.0
No. of rflns. collected	39527
No. of indep. rflns. /R_{int}	6580/0.1391
No. of obsd. rflns. [$I_0 > 2\sigma(I_0)$]	4202
Data / restraints / parameters	6580/0/470
R_1 / wR_2 [$I_0 > 2\sigma(I_0)$]	0.0584/0.1155
R_1 / wR_2 (all data)	0.1123/0.1287
GOF (on F^2)	1.029
Largest diff. peak and hole (e $Å^{-3}$)	0.50/−0.38
CCDC No.	2368460

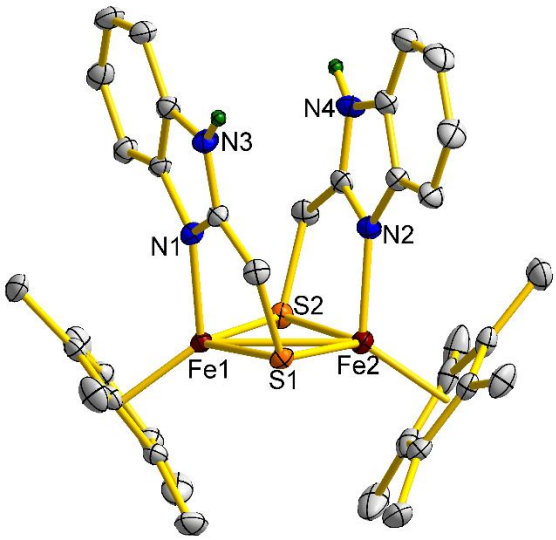

Figure S1. ORTEP diagram of **1**·MeCN. Thermal ellipsoids are shown at 30% probability level. Hydrogen atoms on carbons, one co-crystallized MeCN molecule and two PF_6^- counter anions are omitted for clarity.

Table S4. Selected bond distances and angles for **1**·MeCN.

Distances (Å)			
Fe1−Fe2	2.7892(8)		
Fe1−S1	2.2427(10)	Fe2−S1	2.2178(11)
Fe1−S2	2.2193(11)	Fe2−S2	2.2453(10)
Fe1−N1	1.994(3)	Fe2−N2	1.997(3)
Fe1−Cp*1	1.7744(7)	Fe2−Cp*2	1.7817(7)
Angles (°)			
Fe1−S1−Fe2	77.41(3)	Fe1−S2−Fe2	77.32(3)
Torsion angles (°)			
S2−Fe2Fe1−S1	173.75(5)		
Dihedral angle (°)			
Cp*1∠Cp*2	73.3(2)	Ph1∠Ph2	12.9(1)

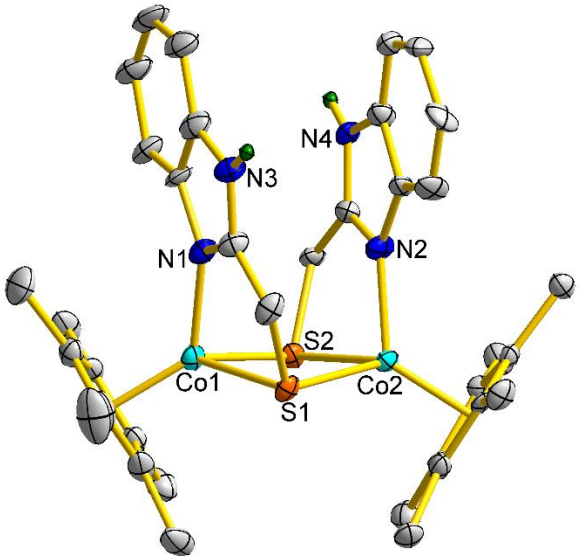

Figure S2. ORTEP diagram of **2**·2CH_2Cl_2. Thermal ellipsoids are shown at 30% probability level. Hydrogen atoms on carbons, two co-crystallized CH_2Cl_2 molecules and two PF_6^- counter anions are omitted for clarity.

Table S5. Selected bond distances and angles for **2**·2CH_2Cl_2.

Distances (Å)			
Co1···Co2	3.321(2)		
Co1−S1	2.259(2)	Co2−S1	2.262(2)
Co1−S2	2.280(2)	Co2−S2	2.271(2)
Co1−N1	1.958(7)	Co2−N2	1.941(7)
Co1−Cp*1	1.696(2)	Co2−Cp*2	1.696(1)
Angles (°)			
Co1−S1−Co2	94.56(9)	Co1−S2−Co2	93.73(8)
Torsion angles (°)			
S2−Co2Co1−S1	163.2(1)		
Dihedral angle (°)			
Cp*1∠Cp*2	64.5(3)	Ph1∠Ph2	2.5(3)

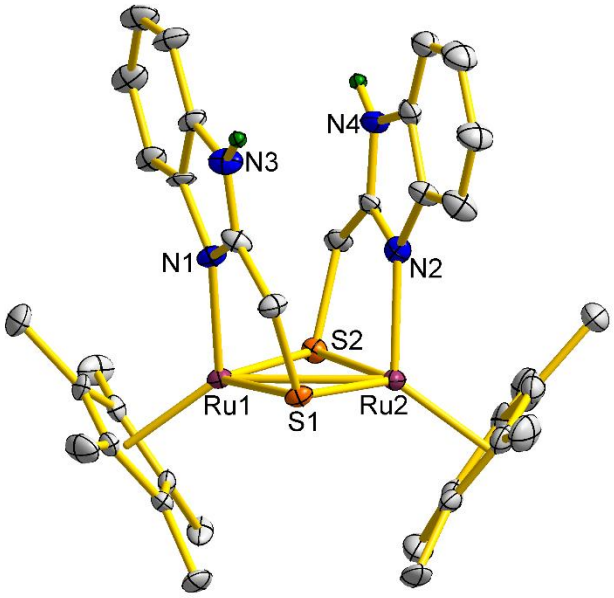

Figure S3. ORTEP diagram of *syn*-**3**·CH_2Cl_2. Thermal ellipsoids are shown at 30% probability level. Hydrogen atoms on carbons, one co-crystallized CH_2Cl_2 molecule and two PF_6^- counter anions are omitted for clarity.

Table S6. Selected bond distances and angles for *syn*-**3**·CH_2Cl_2.

Distances (Å)			
Ru1−Ru2	2.8269(14)		
Ru1−S1	2.306(3)	Ru2−S1	2.310(3)
Ru1−S2	2.311(3)	Ru2−S2	2.317(3)
Ru1−N1	2.118(10)	Ru2−N2	2.101(10)
Ru1−Cp*1	1.8719(9)	Ru2−Cp*2	1.8718(11)
Angles (°)			
Ru1−S1−Ru2	75.54(10)	Ru1−S2−Ru2	75.29(10)
Torsion angles (°)			
S2−Ru1Ru2−S1	173.9(2)		
Dihedral angle (°)			
Cp*1∠Cp*2	74.8(5)	Ph1∠Ph2	8.8(4)

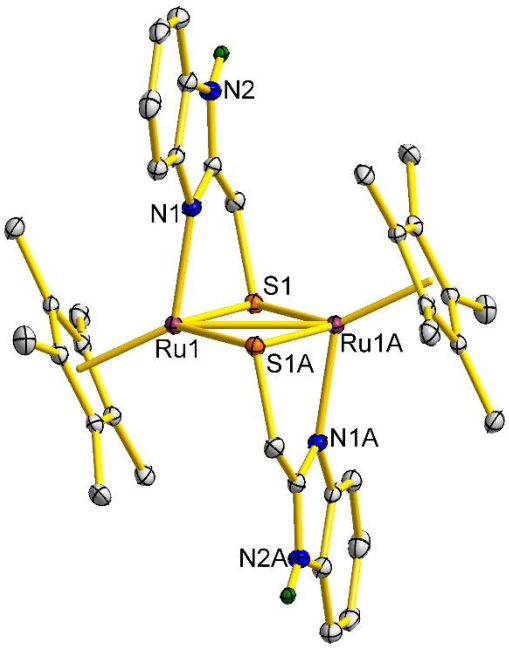

Figure S4. ORTEP diagram of *anti*-**3**·2MeCN. Thermal ellipsoids are shown at 30% probability level. Hydrogen atoms on carbons, two co-crystallized MeCN molecules and two PF_6^- counter anions are omitted for clarity.

Table S7. Selected bond distances and angles for *anti*-**3**·2MeCN.

Distances (Å)			
Ru1−Ru2	2.8339(7)		
Ru1−S1	2.3051(11)	Ru1A−S1	2.3070(11)
Ru1−S1A	2.3070(11)	Ru1A−S1A	2.3051(11)
Ru1−N1	2.106(3)	Ru1A−N1A	2.106(3)
Ru1−Cp*1	1.8665(4)	Ru1A−Cp*1A	1.8665(4)
Angles (°)			
Ru1−S1−Ru1A	75.82(3)		
Torsion angles (°)			
S2−Ru1Ru1A−S1	180.00(5)		
Dihedral angle (°)			
Cp*1∠Cp*1A	0.0(2)	Ph1∠Ph2	0.0(2)

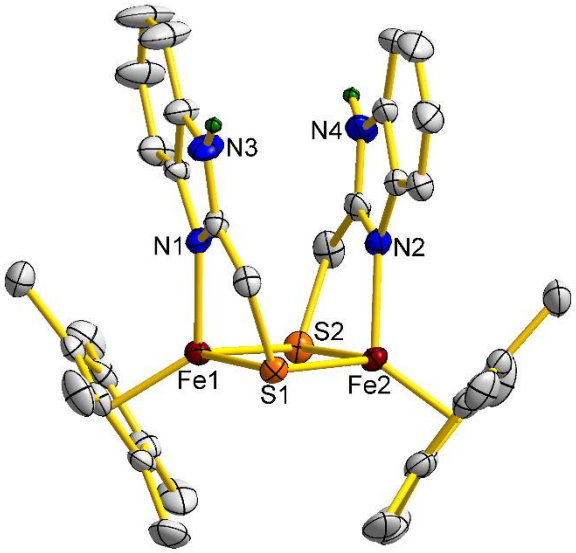

Figure S5. ORTEP diagram of **4**. Thermal ellipsoids are shown at 30% probability level. Hydrogen atoms on carbons and one PF_6^- counter anion are omitted for clarity.

Table S8. Selected bond distances and angles for **4**.

Distances (Å)			
Fe1···Fe2	3.0494(8)		
Fe1−S1	2.2727(12)	Fe2−S1	2.2419(12)
Fe1−S2	2.2489(13)	Fe2−S2	2.2729(12)
Fe1−N1	2.001(3)	Fe2−N2	1.998(3)
Fe1−Cp*1	1.7413(5)	Fe2−Cp*2	1.7360(6)
Angles (°)			
Fe1−S1−Fe2	84.97(4)	Fe1−S2−Fe2	84.81(4)
Torsion angles (°)			
S2−Fe2Fe1−S1	176.74(6)		
Dihedral angle (°)			
Cp*1∠Cp*2	70.4(2)	Ph1∠Ph2	7.7(2)

IV. NMR Spectra

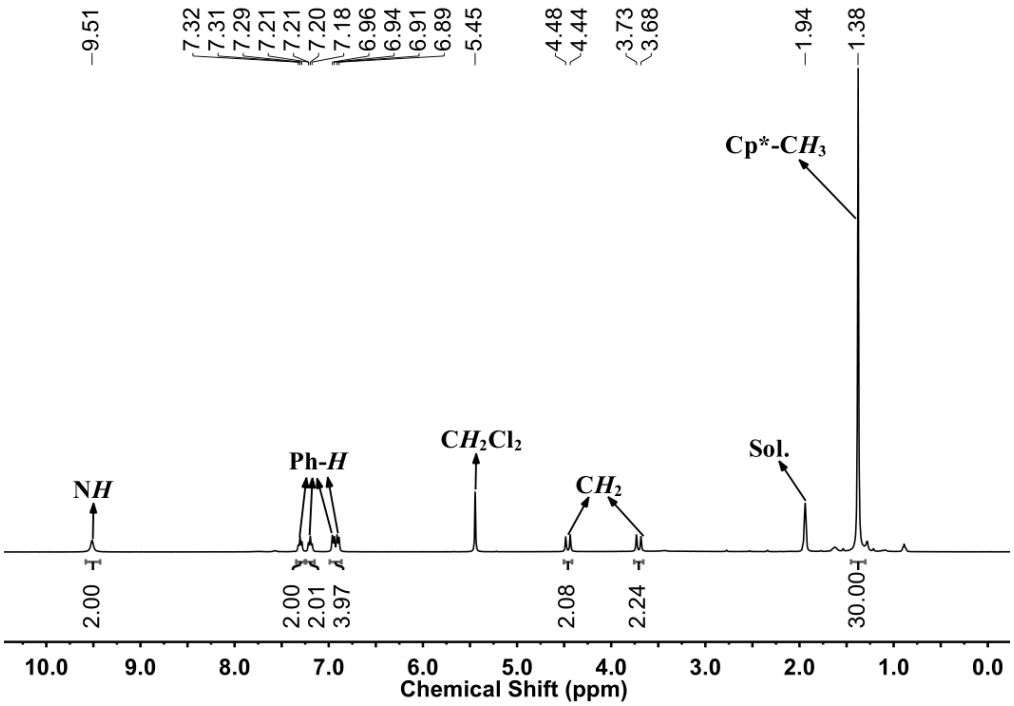

Figure S6. ^{1}H NMR spectrum of **1** in CD_3CN.

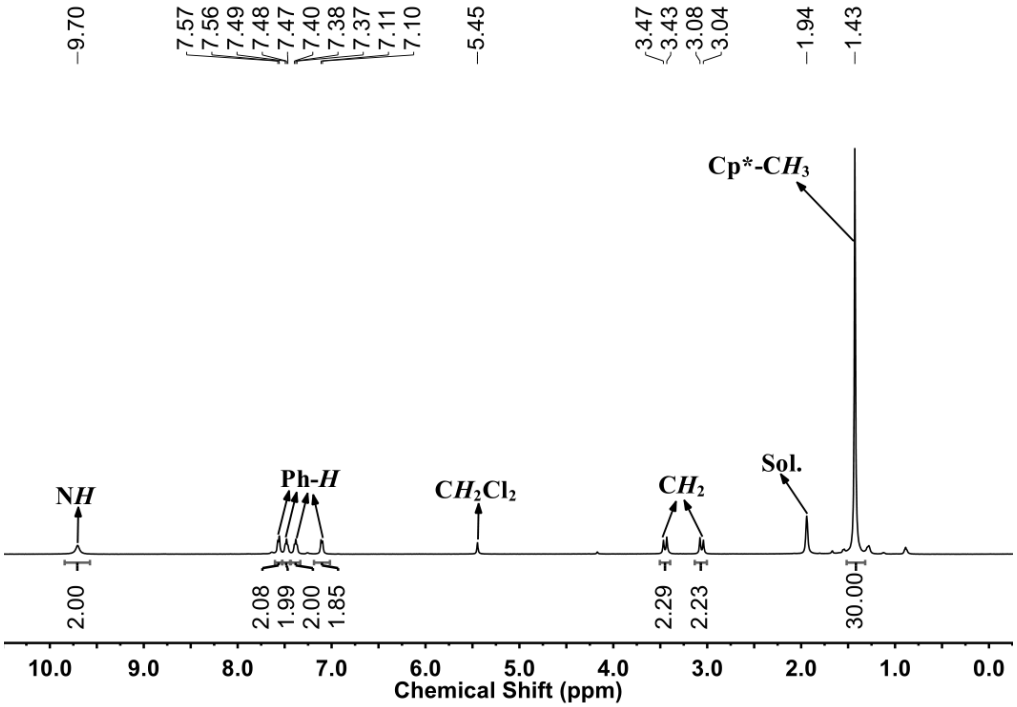

Figure S7. ^{1}H NMR spectrum of **2** in CD_3CN.

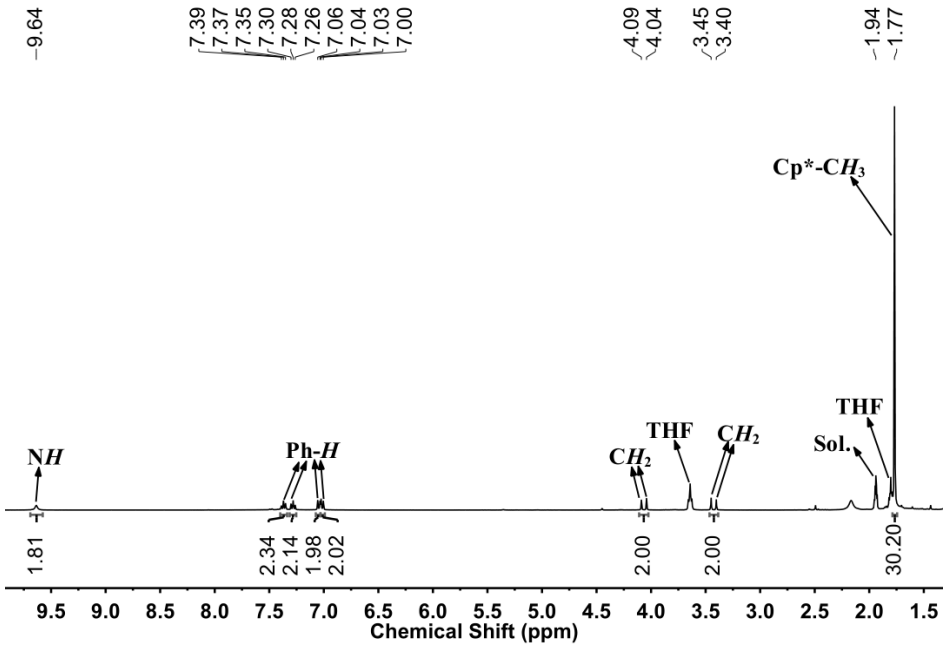

Figure S8. ^{1}H NMR spectrum of *syn*-**3** in CD_3CN.

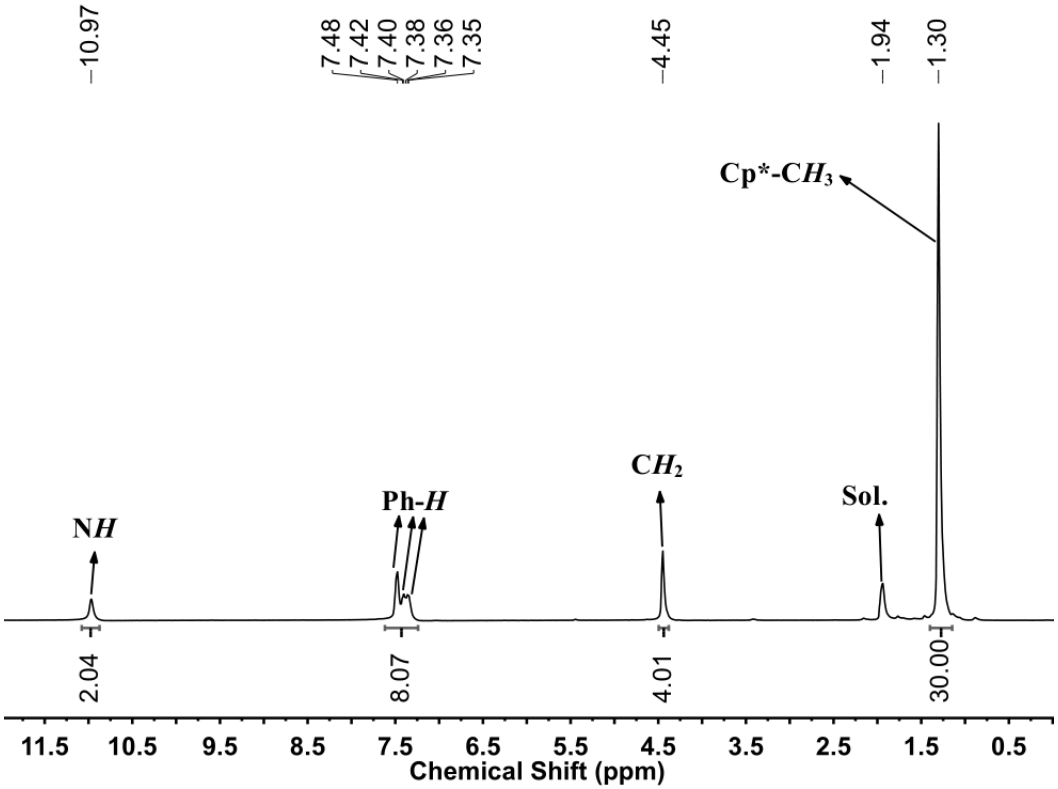

Figure S9. ^{1}H NMR spectrum of *anti*-**3** in CD_3CN.

V. IR Spectra

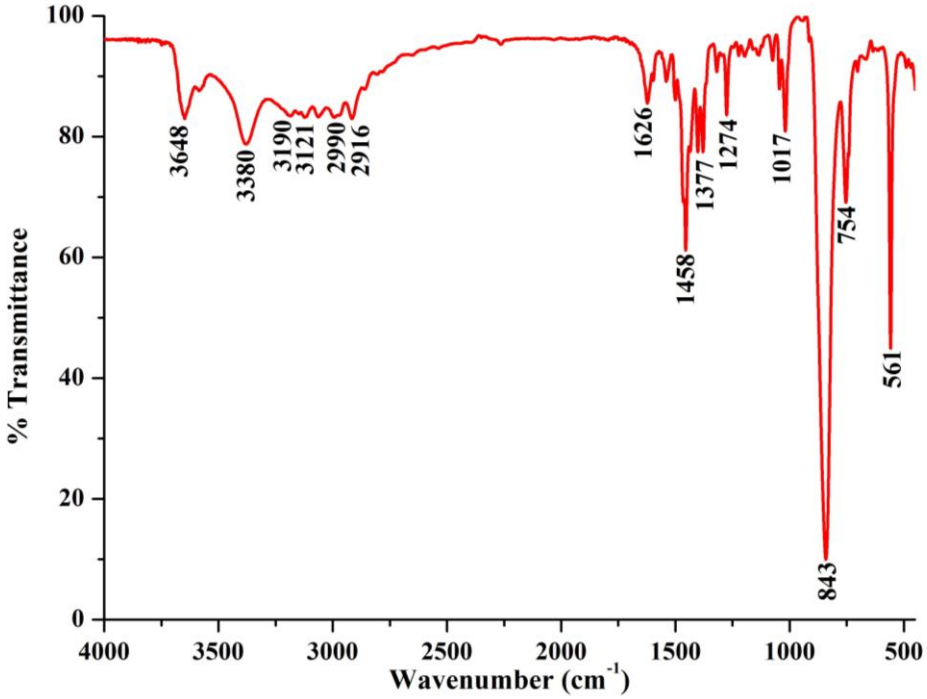

Figure S10. IR spectrum (Film) of **1**.

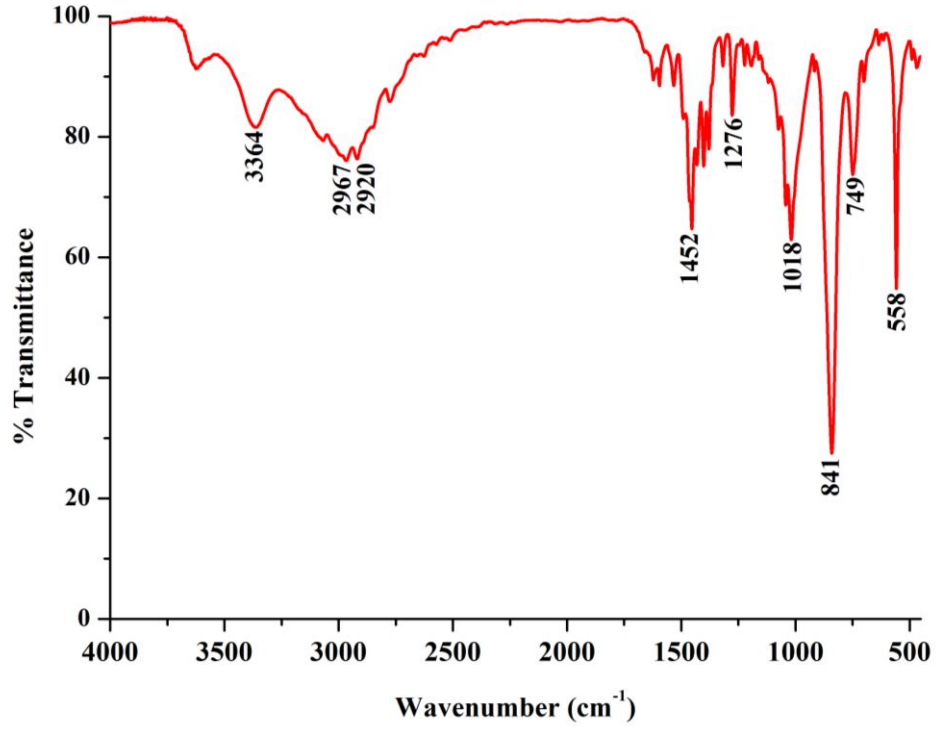

Figure S11. IR spectrum (Film) of **2**.

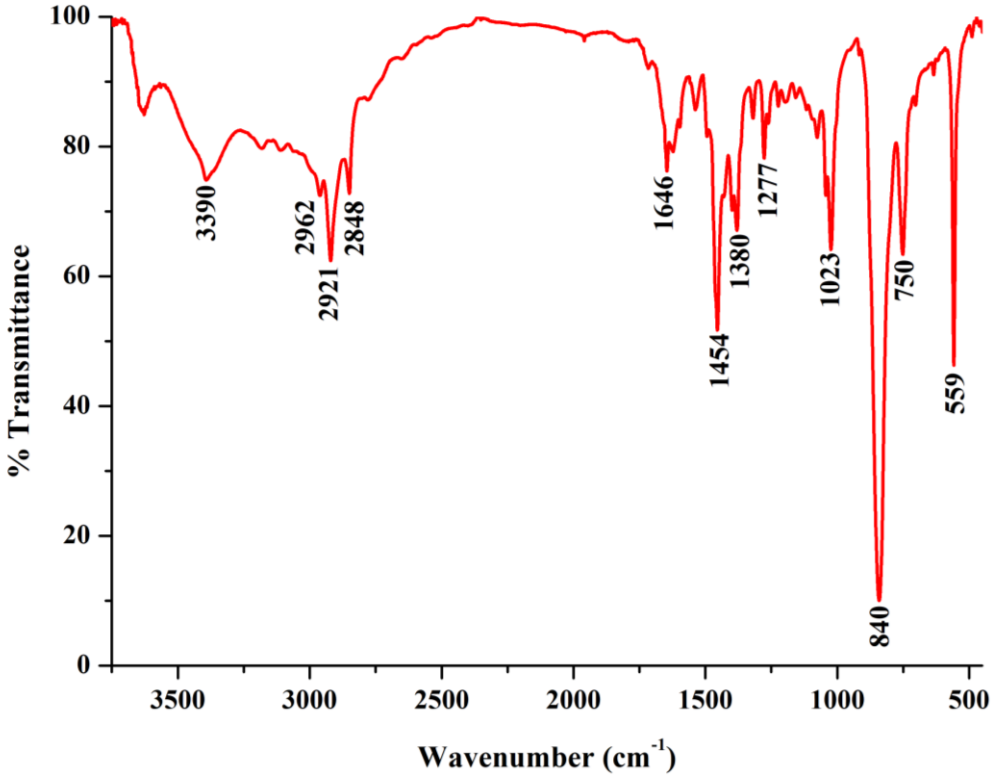

Figure S12. IR spectrum (Film) of *syn*-**3**.

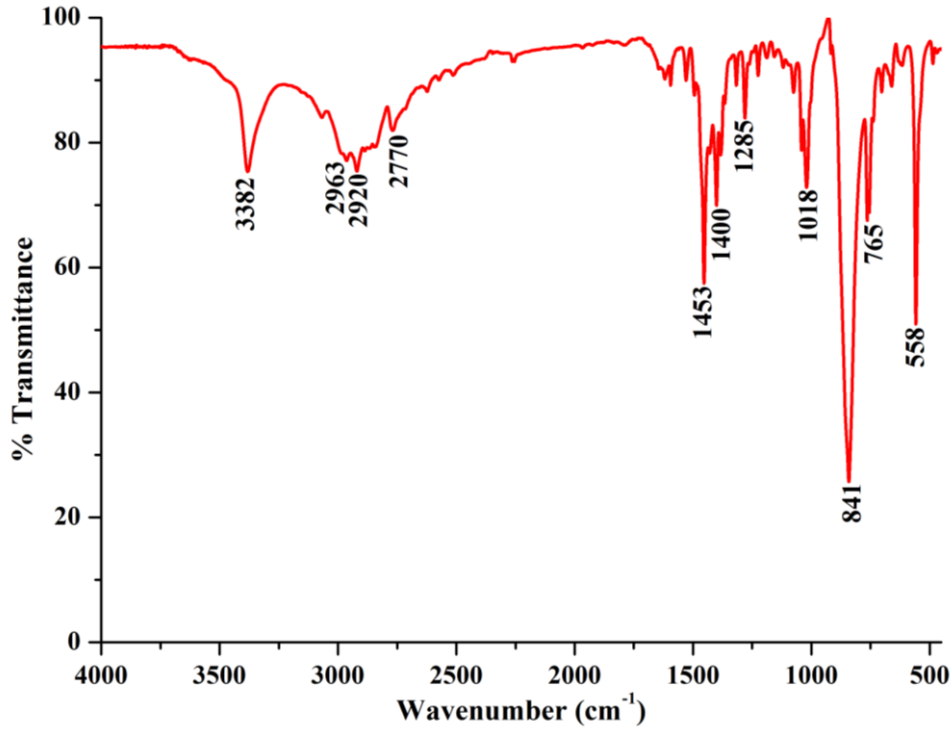

Figure S13. IR spectrum (Film) of *anti*-**3**.

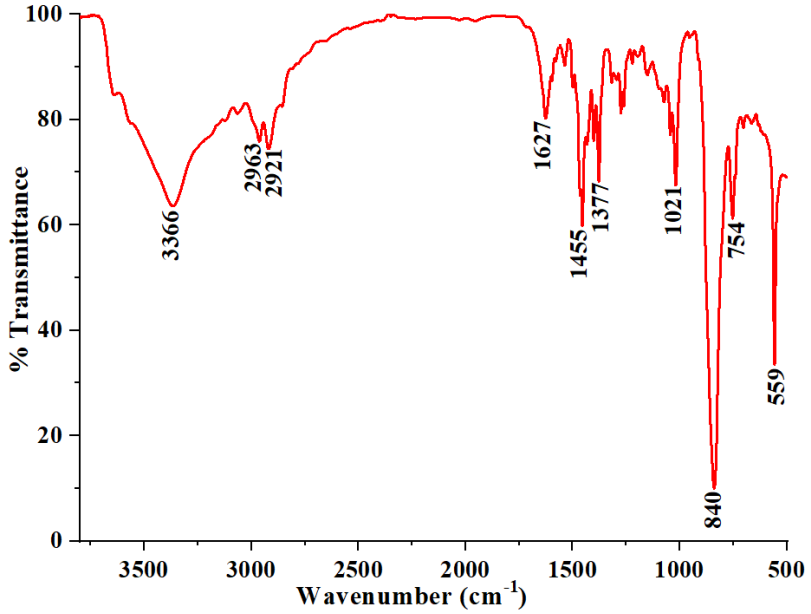

Figure S14. IR spectrum (Film) of **4**.

VI. ESI High-resolution Mass Spectra

(a)

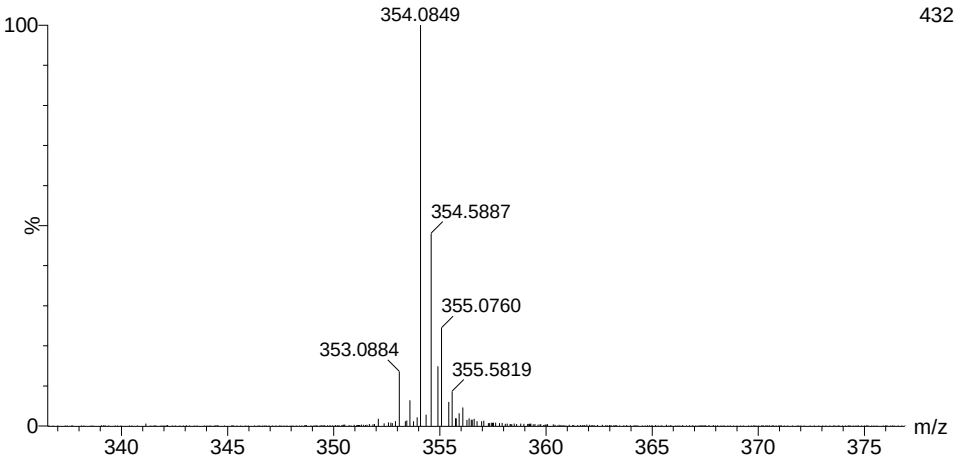

(b)

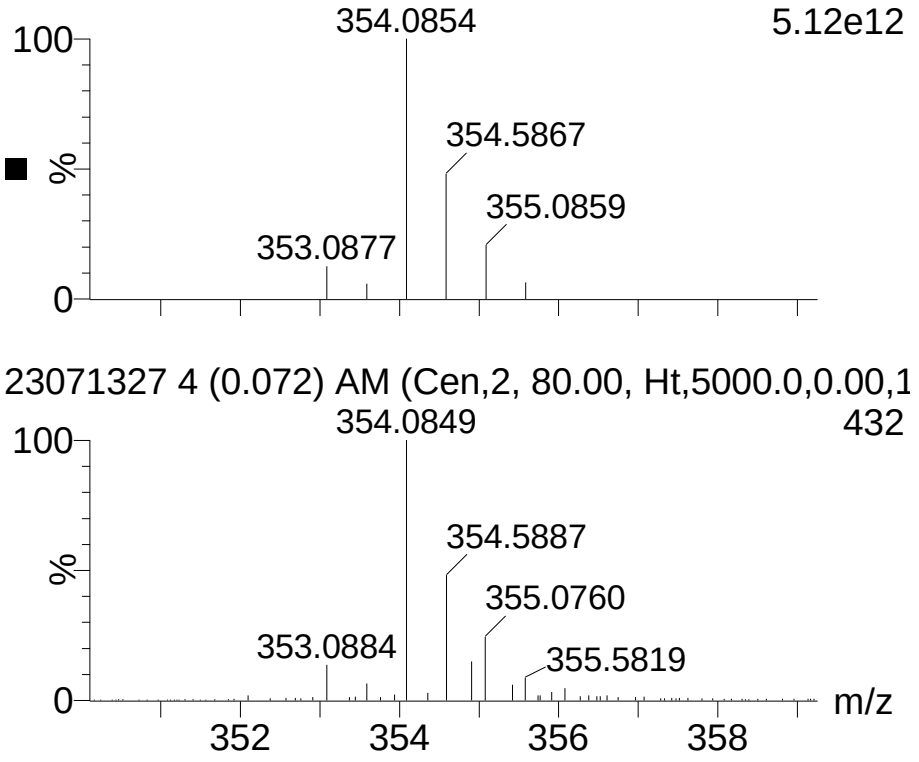

Figure S15. ESI-HRMS of **1** in CH_2Cl_2.

(a) The signal at *m/z* 354.0849 corresponds to $[\mathbf{1}–2(PF_6)]^{2+}$.

(b) Calculated isotopic distribution for $[\mathbf{1}–2(PF_6)]^{2+}$ (upper) and the amplifying experimental diagram for $[\mathbf{1}–2(PF_6)]^{2+}$ (bottom).

(a)

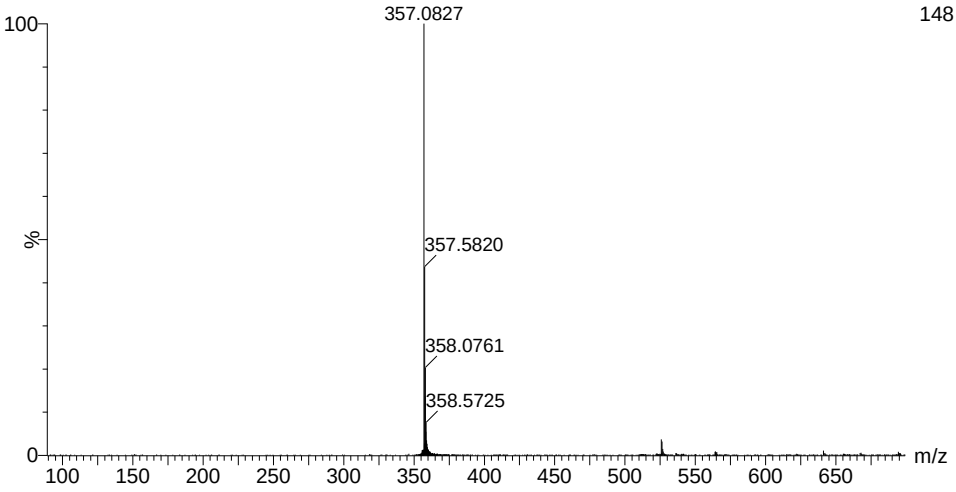

(b)

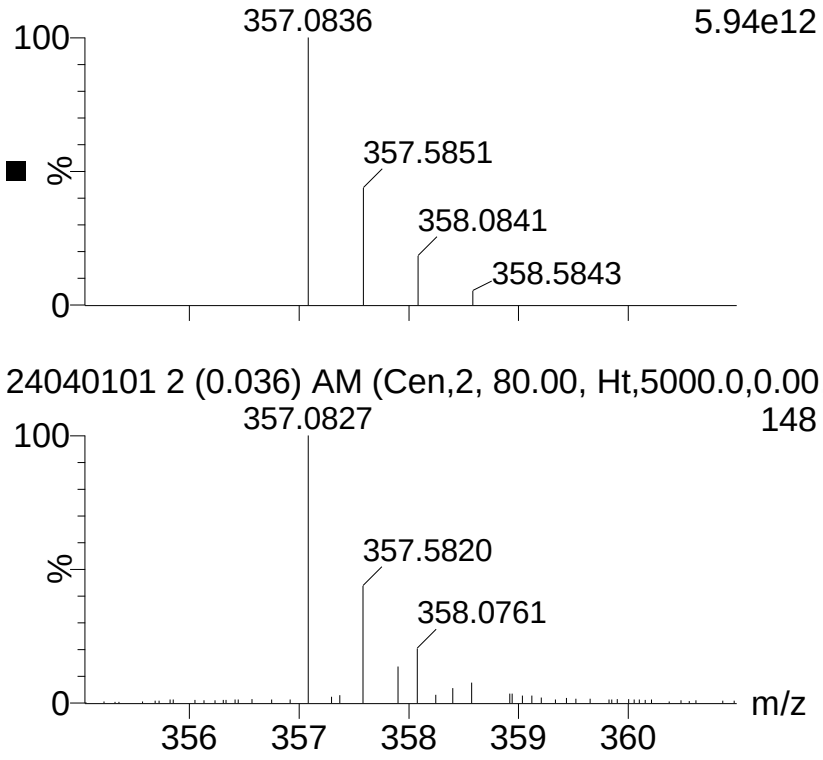

Figure S16. ESI-HRMS of **2** in CH_2Cl_2.

(a) The signal at *m/z* 357.0827 corresponds to $[\mathbf{2}–2(PF_6)]^{2+}$.

(b) Calculated isotopic distribution for $[\mathbf{2}–2(PF_6)]^{2+}$ (upper) and the amplifying experimental diagram for $[\mathbf{2}–2(PF_6)]^{2+}$ (bottom).

(a)

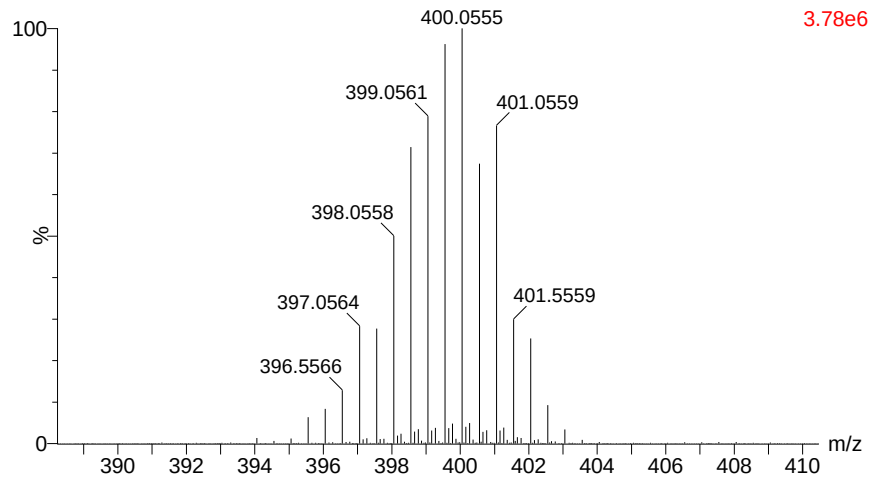

(b)

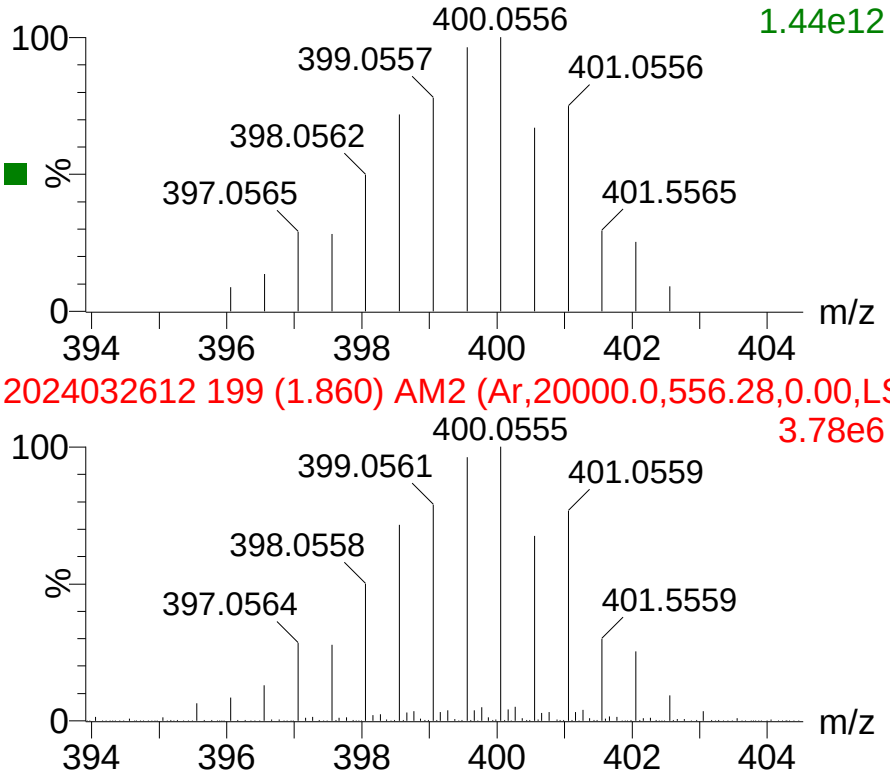

Figure S17. ESI-HRMS of **3** in CH_2Cl_2.

(a) The signal at *m/z* 400.0555 corresponds to $[\mathbf{3}–2(PF_6)]^{2+}$.

(b) Calculated isotopic distribution for $[\mathbf{3}–2(PF_6)]^{2+}$ (upper) and the amplifying experimental diagram for $[\mathbf{3}–2(PF_6)]^{2+}$ (bottom).

(a)

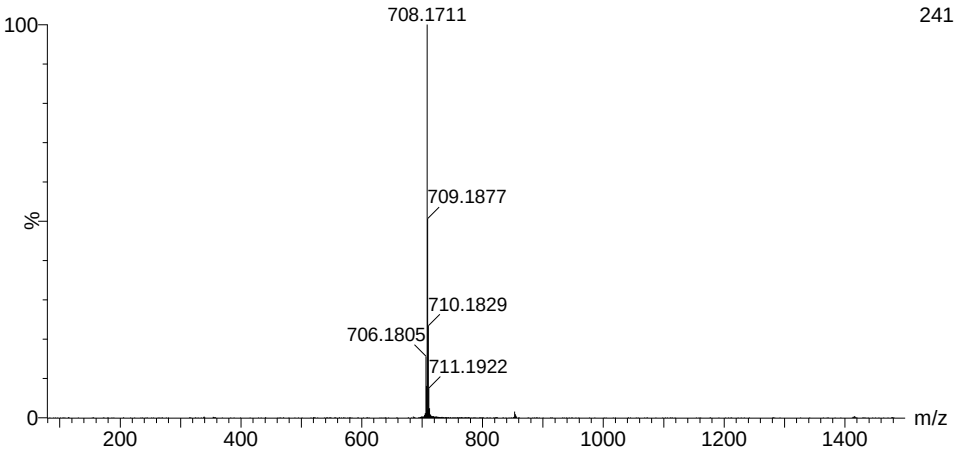

(b)

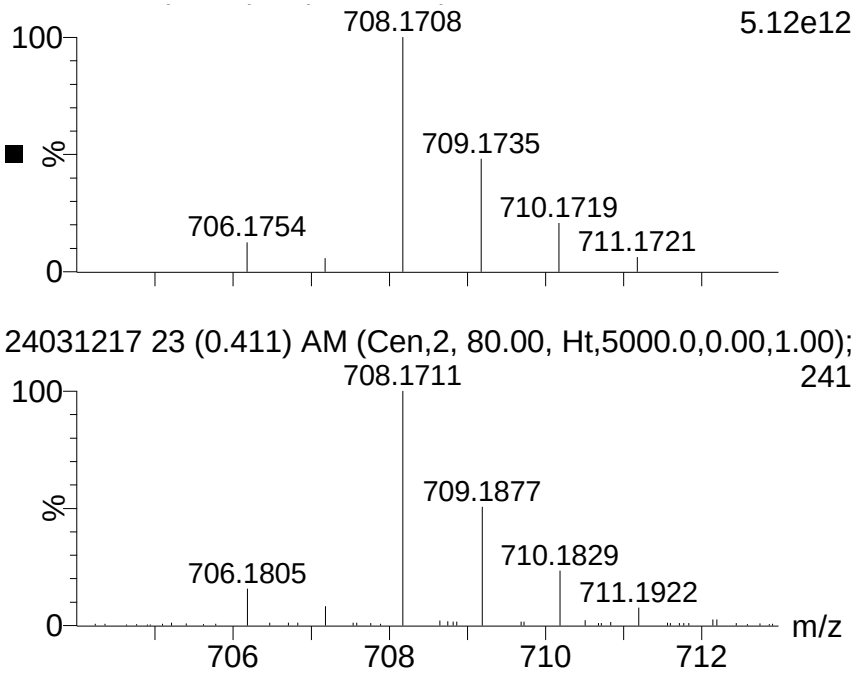

Figure S18. ESI-HRMS of **4** in CH_2Cl_2.

(a) The signal at *m/z* 708.1711 corresponds to $[\mathbf{4}–PF_6]^+$.

(b) Calculated isotopic distribution for $[\mathbf{4}–PF_6]^+$ (upper) and the amplifying experimental diagram for $[\mathbf{4}–PF_6]^+$ (bottom).

VII. Cyclic Voltammograms

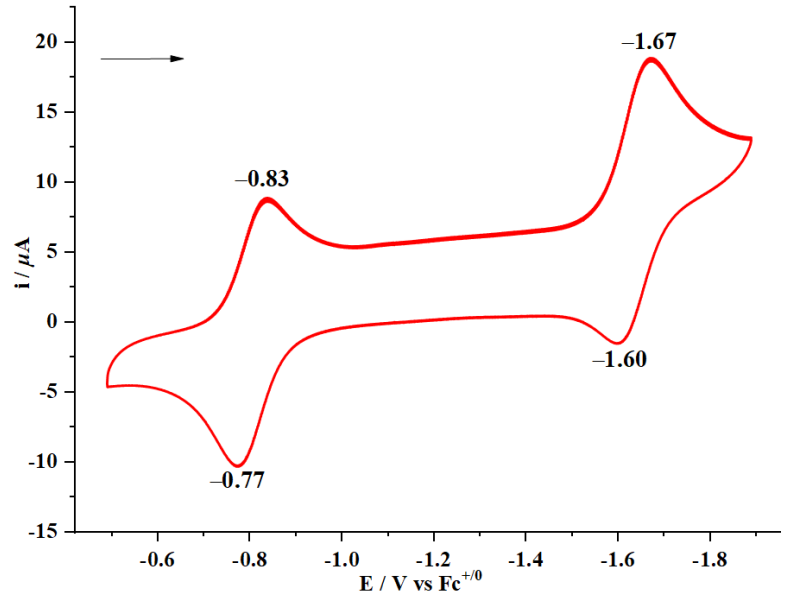

Figure S19. The cyclic voltammogram of **1** (1 mM) in MeCN recorded at a scan rate of 100 mV s^{-1} with 0.1 M $^{n}Bu_4NPF_6$ as supporting electrolyte under a nitrogen atmosphere at room temperature. All potentials are referenced versus $Fc^{+/0}$ redox couple.

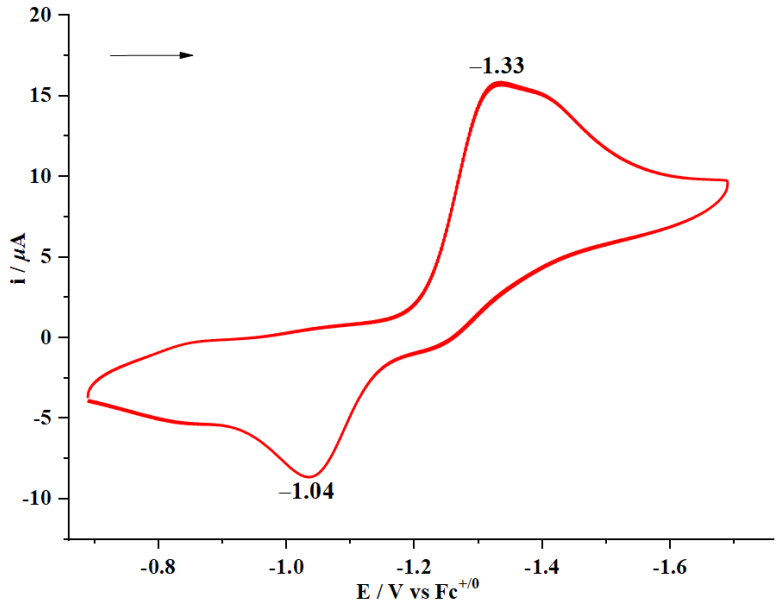

Figure S20. The cyclic voltammogram of **2** (1 mM) in MeCN recorded at a scan rate of 100 mV s^{-1} with 0.1 M $^{n}Bu_4NPF_6$ as supporting electrolyte under a nitrogen atmosphere at room temperature. All potentials are referenced versus $Fc^{+/0}$ redox couple.

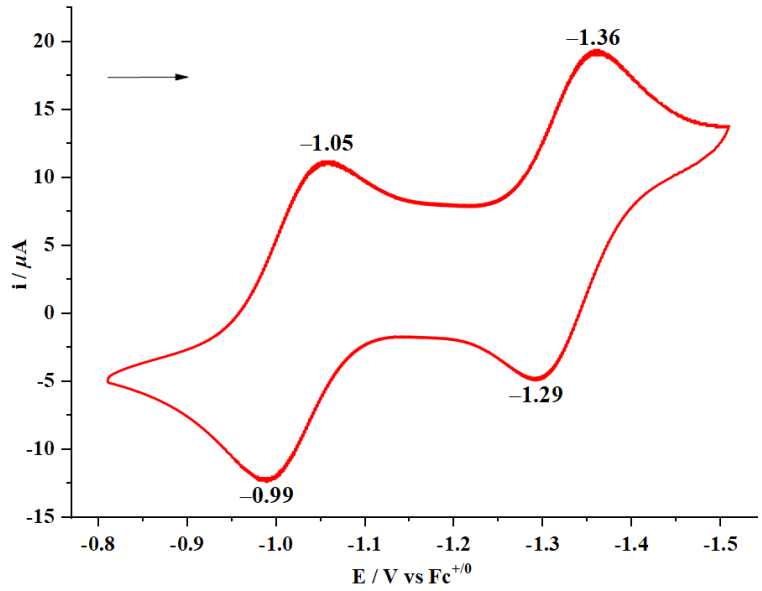

Figure S21. The cyclic voltammogram of **3** (1 mM) in MeCN recorded at a scan rate of 100 mV s^{-1} with 0.1 M $^{n}Bu_4NPF_6$ as supporting electrolyte under a nitrogen atmosphere at room temperature. All potentials are referenced versus $Fc^{+/0}$ redox couple.

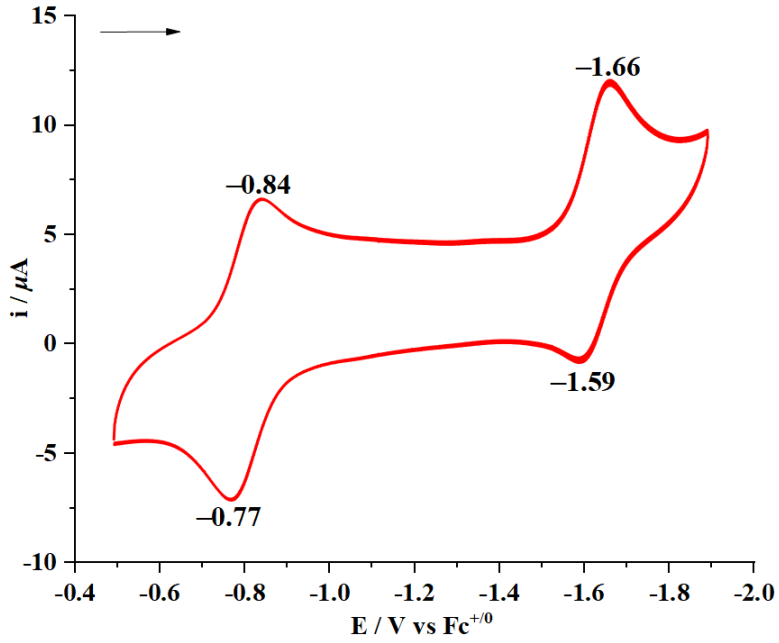

Figure S22. The cyclic voltammogram of **4** (1 mM) in MeCN recorded at a scan rate of 100 mV s^{-1} with 0.1 M $^{n}Bu_4NPF_6$ as supporting electrolyte under a nitrogen atmosphere at room temperature. All potentials are referenced versus $Fc^{+/0}$ redox couple.

VIII. *In situ* ^{1}H NMR Spectra

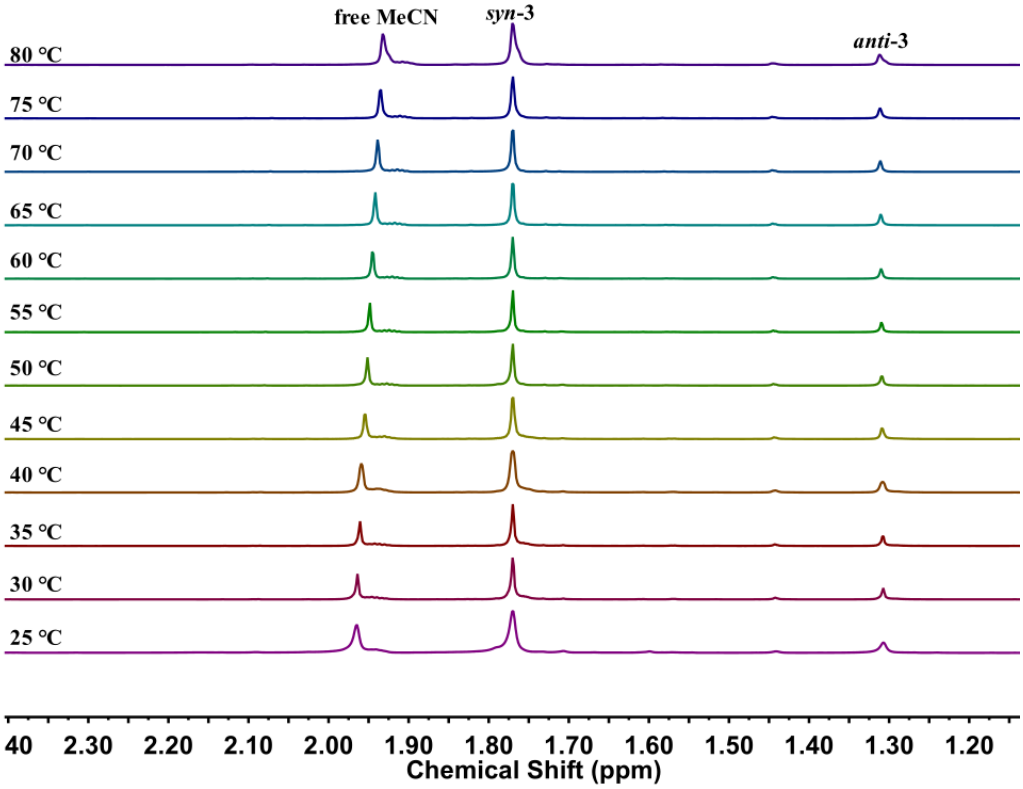

Figure S23. ^{1}H NMR spectra for the mixture of complexes *syn*-**3** and *anti*-**3** in CD_3CN at differnet temperatures.

IX. UV/vis Spectra

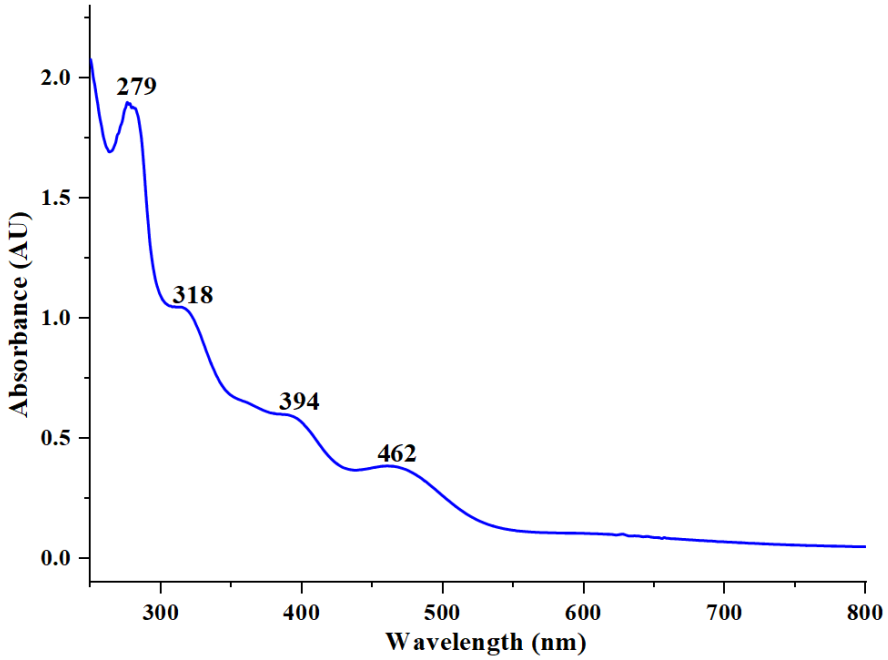

Figure S24. UV/vis spectrum of **1** in MeCN (0.1 mM) at 298 K.

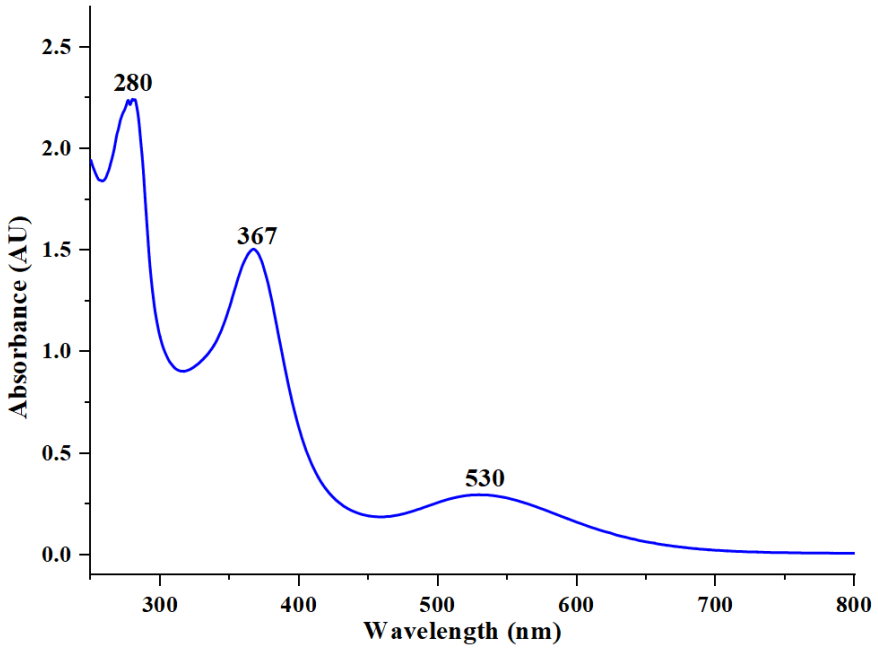

Figure S25. UV/vis spectrum of **2** in MeCN (0.1 mM) at 298 K.

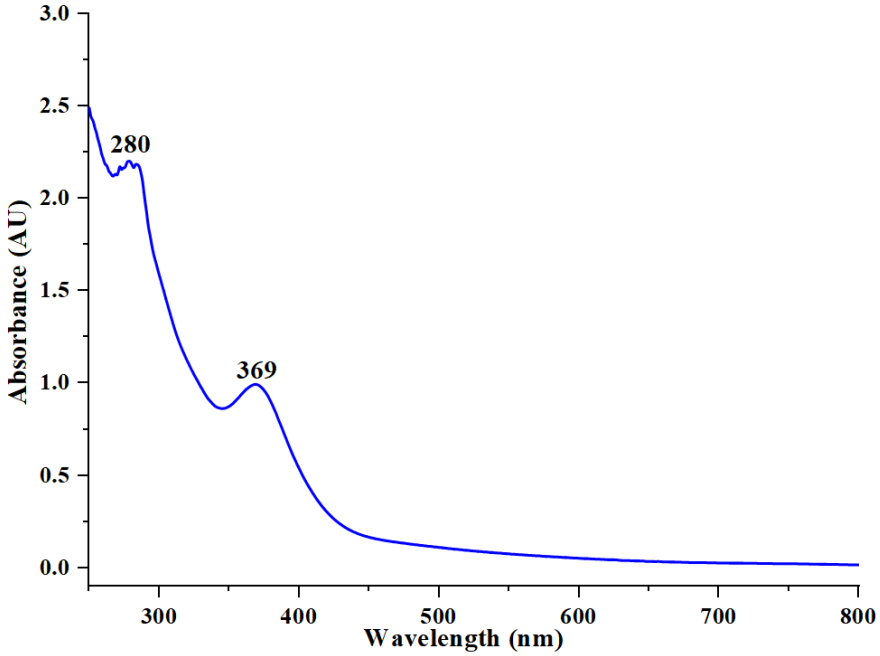

Figure S26. UV/vis spectrum of *syn*-**3** in MeCN (0.1 mM) at 298 K.

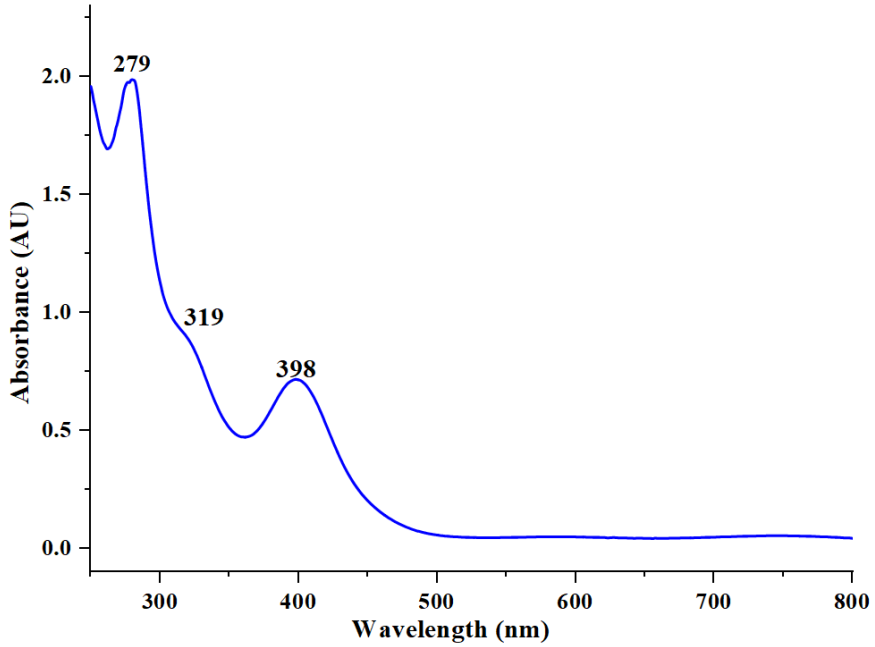

Figure S27. UV/vis spectrum of *anti*-**3** in MeCN (0.1 mM) at 298 K.

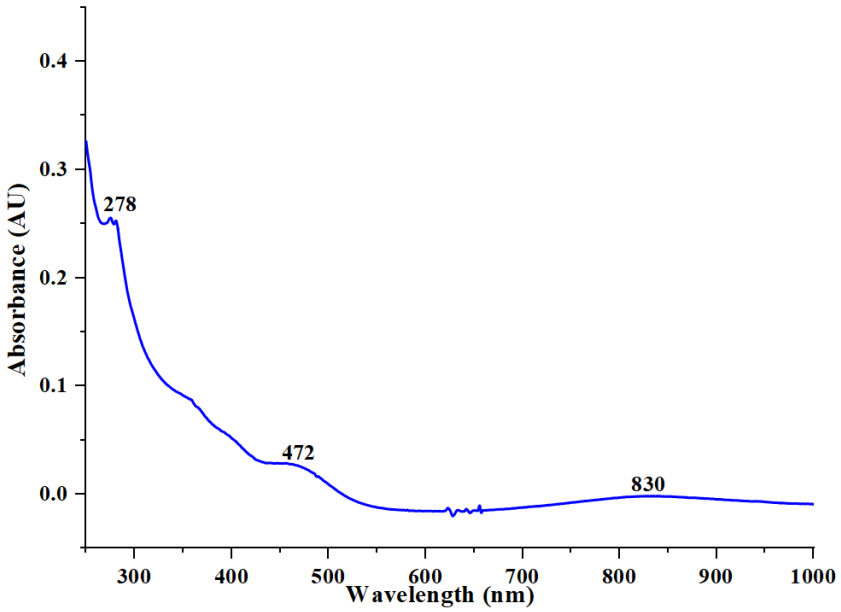

Figure S28. UV/vis spectrum of **4** in MeCN (0.1 mM) at 298 K.

X. Computational Details

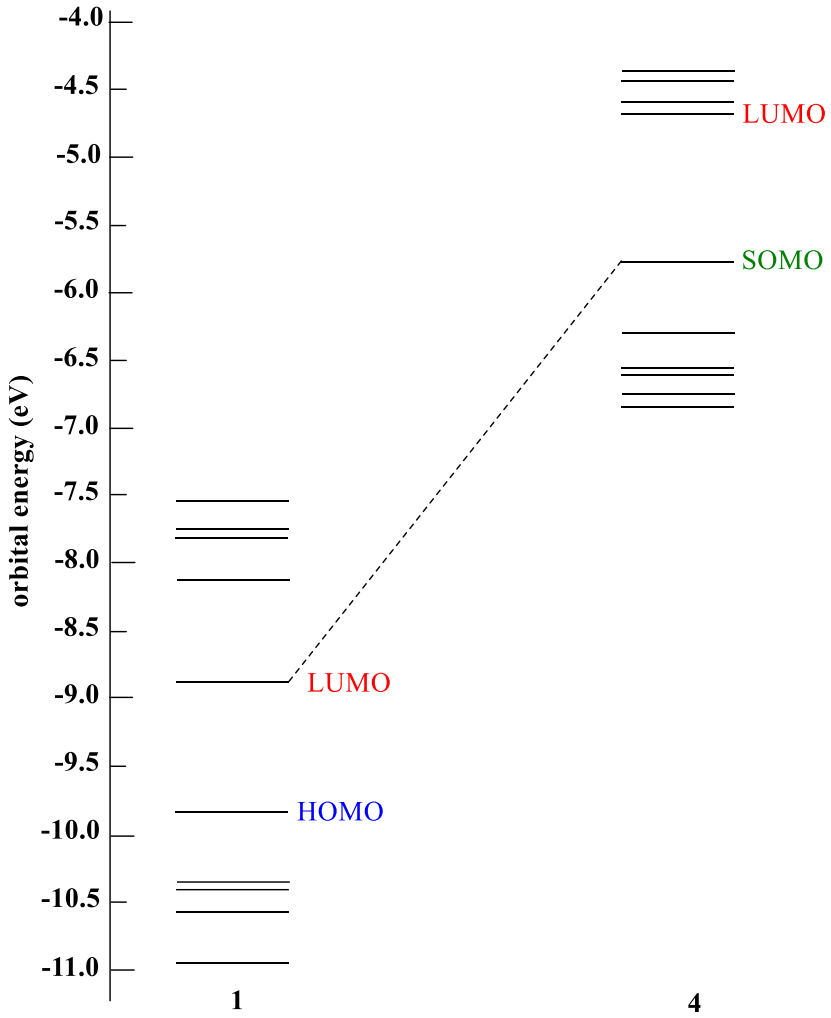

Figure S29. Orbital diagram and relevant molecular orbitals of **1** and **4** calculated at the PBE/TZVP level of theory on the geometries optimized using the PBE/TZVP scheme.

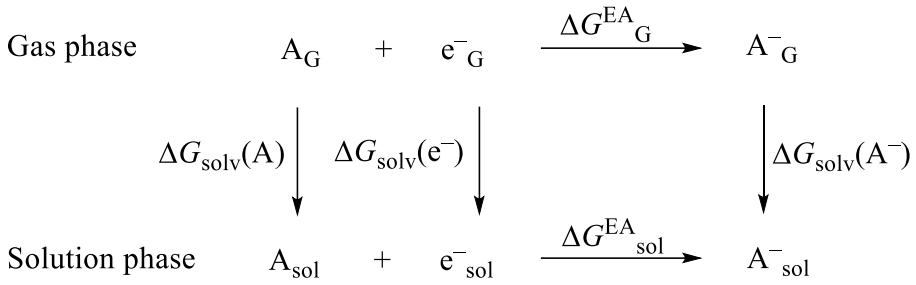

Scheme 1. Thermodynamic cycle used for the calculations of reduction potentials.

The redox potential of a given electron coupling reaction in solution was calculated by using theGibbs free energy change (ΔG^{EA}_{sol}).

$$E^{\circ} = -\Delta G^{EA}_{sol}/F \quad (1)$$

Where F represents the Faraday constant and ΔG^{EA}_{sol} was computed with the thermodynamic cycle in **Scheme 1**.

$$\Delta G^{EA}_{sol} = \Delta G^{EA}_{G} + \Delta G_{sol}(A^-) - \Delta G_{sol}(AH) - \Delta G_{sol}(e^-) \quad (2)$$

Since the accurate solvation energy of a single electron is difficult to determine experimentally, the relative redox potential was calculated with respect to the NHE in acetonitrile for which a shift of −4.48 V was used as suggested by Cramer and Truhlar.[22,23]

$$E^{o}(NHE) = -(\Delta G^{EA}_{G} + \Delta G_{sol}(A^-) - \Delta G_{sol}(AH))/F - 4.48 \quad (3)$$

XI. References

1. H. P. Berends and D. W. Stephan, *Inorg. Chim. Acta*, 1984, **93**, 173−178.
2. D. Catheline and D. Astruc, *Organometallics*, 1984, **3**, 1094–1100.
3. S. A. Frith and J. L. Spencer, *Inorg. Synth.*, 1985, **23**, 15−17.
4. P. J. Fagan, M. D. Ward and J. C. Calabrese, *J. Am. Chem. Soc.*, 1989, **111**, 1698−1719.
5. I. S. Weitz and M. Rabinovitz, *J. Chem. Soc. Perkin Trans.*, 1993, **1**, 117−120.
6. B. W. Carlson, L. L. Miller, P. Neta and J. Grodkowski, *J. Am. Chem. Soc.*, 1984, **106**, 7233–7239.
7. D. F. Evans, *J. Chem. Soc.*, 1959, 2003−2005.
8. E. M. Schubert, *J. Chem. Educ.*, 1992, **69**, 62.
9. C. Piguet, *J. Chem. Educ.*, 1997, **74**, 815−816.
10. G. A. Bain and J. F. Berry, *J. Chem. Educ.*, 2008, **85**, 532−536.
11. G. M. Sheldrick, Institute for Inorganic Chemistry, University of Göttingen, Germany, 1996.
12. G. M. Sheldrick, SHELXL-2014, Program for refinement of crystal structures, University of Göttingen, Germany, 2014.
13. G. M. Sheldrick, SHELXS-2014, Program for solution of crystal structures, University of Göttingen, Germany, 2014.
14. L. Palatinus and G. Chapuis, *J. Appl. Crystallogr.*, 2007, **40**, 786−790.
15. O. V. Dolomanov, L. J. Bourhis, R. J. Gildea, J. A. K. Howard and H. Puschmann, *J. Appl. Crystallogr.*, 2009, **42**, 339−341.
16. G. M. Sheldrick, *Acta Crystallogr., Sect. A: Found. Adv.*, 2015, **71**, 3−8.
17. A. D. Becke, *Phys. Rev. A.*, 1988, **38**, 3098−3100.
18. J. P. Perdew, K. Burke and M. Ernzerhof, *Phys. Rev. Lett.*, 1996, **77**, 3865−3868.
19. A. Schäfer, C. Huber and R. Ahlrichs, *J. Chem. Phys.*, 1994, **100**, 5829−5835.
20. K. Eichkorn, O. Treutler, H. Öhm, M. Häser and R. Ahlrichs, *Chem. Phys. Lett.*, 1995, **240**, 283−290.
21. S. Grimme, S. Ehrlich and L. Goerigk, *J. Comput. Chem.*, 2011, **32**, 1456−1465.
22. C. P. Kelly, C. J. Cramer and D. G. Truhlar, *J. Phys. Chem. B*, 2007, **111**, 408−422.
23. J. Song, E. L. Klein, F. Neese and S. Ye, *Inorg. Chem.*, 2014, **53**, 7500−7507.